ROYAL SOCIETY
OF CHEMISTRY

PAPER
Željka Fiket *et al.*
Stability of nanodiamonds and carbon dots in aqueous
environments: insights into aggregation behavior and
additive influence

PAPER

Check for updates

Stability of nanodiamonds and carbon dots in aqueous environments: insights into aggregation behavior and additive influence

Željka Fiket, †*[a] Maja Dutour Sikirić, †[b] Darija Gal,[c] Marija Petrović,[a] Vida Strasser,[b] Veronika Kovač,[d] Sanja Frka,[a] Neda Vdović[a] and Binoy Saikia[e]

This study investigated the stability of carbon-based nanoparticles, specifically carbon dots (CDs) and nanodiamonds (NDs), in model systems designed to mimic a natural water environment. Dynamic light scattering (DLS) and zeta potential measurements were performed to evaluate particle size distribution, surface charge and their stability both as standalone nanoparticles and in the presence of additives such as bovine serum albumin (BSA), dextran sulfate sodium salt (DSS), fulvic acid (FA) and natural organic matter (NOM). The results showed significant differences in stability between CDs and NDs, with CDs showing a tendency to aggregate, while NDs exhibited higher stability under different conditions. The addition of BSA, FA and NOM significantly affected the zeta potential, although the ND suspensions remained stable under acidic conditions. Conversely, DSS had minimal effects on the zeta potential, resulting in the stabilization effect in Milli-Q water. In NaCl suspensions, addition of additives resulted in aggregation, with the exception of NOM, which improved the stability of NDs under alkaline conditions. These results improve our understanding of the environmental behaviour of carbon-based nanoparticles and highlight the role of environmental factors and additives in their stability. This knowledge is crucial not only for evaluating their behaviour and potential impact on the aquatic environment but also for developing novel technologies that exploit their unique properties for sustainable and innovative applications.

Environmental significance

Carbon-based nanomaterials are increasingly used in various applications, but their interactions with environmental components are still poorly understood. Upon release into aqueous environments, these nanomaterials inevitably interact with organic matter and biomolecules, affecting their stability, reactivity and potential impact on the environment. This study provides new insights into the interactions between carbon-based nanomaterials and key environmental components such as proteins, organic matter and fulvic acid, which are critical for predicting their fate in natural waters. Understanding these interactions is important for assessing the environmental risks and benefits of nanomaterials, for developing sustainable nanotechnology and for establishing environmental safety regulations.

1. Introduction

Carbon-based nanomaterials such as fullerenes, carbon nanotubes, graphene and its derivatives, graphene oxide, nanodiamonds, and carbon-based quantum dots have attracted great attention in various fields such as imaging, sensing, therapeutics, energy storage, *etc.* due to their unique physicochemical properties and ultra-small size.[1,2] Carbon dots (CDs) are carbon nanoparticles consisting of carbon quantum dots (CQDs) and graphene quantum dots (GQDs) with a size of less than 10 nm and less than 100 nm, respectively, which are usually synthesized from organic materials by simple and low-cost methods such as laser ablation, electrochemical oxidation, combustion/thermal microwave heating, ultrasonic-assisted synthesis, chemical oxidation, hydrothermal carbonization and pyrolysis.[2,3] These particles can be further tailored by introducing surface defects, adjusting their size, and applying chemical

[a] Division for Marine and Environmental Research, Ruđer Bošković Institute, Zagreb, Croatia. E-mail: zeljka.fiket@irb.hr
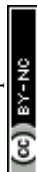*[b] Division of Physical Chemistry, Ruđer Bošković Institute, Zagreb, Croatia*
[c] Department of Chemistry, Faculty of Science, University of Zagreb, Zagreb, Croatia
[d] Department of Chemistry and Biochemistry, Faculty of Food Technology and Biotechnology, University of Zagreb, Zagreb, Croatia
[e] Coal & Energy Division, CSIR-North East Institute of Science & Technology, Jorhat, India
† These authors contributed equally to this work.

3904 | *Environ. Sci.: Nano*, 2025, **12**, 3904–3920

This journal is © The Royal Society of Chemistry 2025

modifications or nitrogen doping to improve their properties.[4] Nanodiamonds, on the other hand, are diamond nanocrystals that possess exceptional diamond properties such as hardness, thermal conductivity, elasticity, and a chemically inert core, as well as nanoparticle properties such as a large surface area, surface functionalization, and biocompatibility.[5] Similar to carbon dots, the surface of nanodiamonds contains numerous dangling ends that can covalently bind to various groups such as hydroxyl (OH), carbonyl (C=O), carboxyl (COOH), *etc.* Moreover, they are susceptible to functionalization and modification due to imperfections in their structure, leading to their widespread use in various fields.[6–9]

Despite their promising applications and decades of research and development into their production and modification, there remains a significant gap in our understanding of how carbon-based nanomaterials behave in aqueous environments,[10] which is particularly critical given their widespread use and potential impact on biological systems and ecosystems.[2] This knowledge gap emphasizes the importance of studying the interactions between nanoparticles and environmental components such as proteins and organic matter. Not only do these interactions inevitably occur when nanoparticles are released into the environment, but they also play an important role in shaping the behavior of nanoparticles in aqueous environments.[9,11–14] For example, albumin-conjugated ND-supported silver nanoparticles have shown strong antimicrobial activity with low toxicity to human cells.[9] Fulvic acid (FA), a component of natural organic matter, has been reported to interact with nanomaterials and can affect their surface properties and environmental behavior.[13,14] Similarly, the adsorption of proteins such as bovine serum albumin (BSA) on ND surfaces has been shown to influence their stability and reactivity.[11,12]

Most studies to date have focused on salinity levels relevant to biological fluids,[15] while only a limited number of studies have examined a broader salinity range of approximately 3.5 to 18 PSU.[12] However, aquatic freshwater systems, including rivers, lakes, wetlands, and marshes, have not been systematically studied in the literature. Given the different environmental conditions and biogeochemical processes in these ecosystems, filling this research gap is crucial for an accurate assessment of the behavior of nanoparticles in natural waters.

Therefore, the main objective of this study was to investigate the behavior and stability of carbon-based nanoparticles, including carbon dots and nanodiamonds, in aqueous model suspensions to better understand their behavior in the aquatic environment. To this end, the following specific objectives were as follows: (a) to analyze the change in the particle size distribution of carbon dots and nanodiamonds in different media (water and aqueous sodium chloride solution) and the latter in the presence of different additives (bovine serum albumin, dextran sulfate sodium salt, fulvic acid, and natural organic material from the Suwannee River), (b) to evaluate the electrophoretic

mobility of these nanoparticles under the same conditions to characterize their surface charge and interaction dynamics, and (c) to determine the optimal pH conditions that ensure the stability of the suspensions of nanoparticles.

2. Materials and methods

2.1. Materials

Two types of carbon-based nanoparticles, carbon dots (CDs) and nanodiamonds (NDs), were used in this study.

The carbon dots (CD1 and CD2) were prepared from two different subbituminous coal sources from Northeast India, and the concentrations of the CDs were about 4.5 mg mL^{-1} and 5.1 mg mL^{-1}, respectively. These carbon quantum dots are composed of carbon nanocrystals with a size of less than 10 nm and their surface is functionalized with COOH, C=O, and O–H groups. The CDs were prepared by a chemical oxidation method using oxidizing agents. Details of the method used to prepare the CDs from the coal samples can be found elsewhere.[3]

The nanodiamond suspensions were prepared from the standard solution of monodispersed nanodiamond particles in water (stock solution, 5 nm average particle size, carboxylated, Sigma-Aldrich, Germany), and the mass concentration of NDs was 10 mg mL^{-1}.

The stability of CD and ND suspensions in water and aqueous sodium chloride solution was investigated, and the latter also in the presence of additives including bovine serum albumin (BSA, Sigma-Aldrich, Germany), dextran sulfate sodium salt (DSS, Sigma-Aldrich, Germany) and reference substances, Suwannee River fulvic acid (FA, 2S101F, IHSS, Georgia, USA) and natural organic material from an aquatic system (NOM, 2R101N, IHSS, Georgia, USA).

2.2. Experimental setup

The experimental setup included the preparation of CD and ND suspensions (15 mg L^{-1}) in Milli-Q (MQ) water and an aqueous NaCl solution (15 mg L^{-1}), which represents the typical electrolyte conditions for river water.

For NDs, additional measurements were performed in suspensions enriched with additives at a final concentration of 50 mg L^{-1}, including BSA, DSS, FA, and NOM. The selected additives represent substances commonly found in natural aquatic systems, both pristine and anthropogenically impacted. Bovine serum albumin was selected as a representative protein,[16] dextran sulfate sodium salt as a model pollutant or inflammatory agent,[17] and natural organic matter and fulvic acid as major components of dissolved organic matter. The concentrations of these additives were defined based on the literature values. Dissolved organic matter (DOM), which includes fulvic acid and proteins, has been documented at 1–10 mg L^{-1} in rivers and 1–50 mg L^{-1} in lakes,[18,19] with concentrations exceeding 50 mg L^{-1} in wastewater.[20] To avoid concentration-dependent effects, the selected concentrations of all additives were kept at a fixed level (50 mg L^{-1}) throughout the study.

This journal is © The Royal Society of Chemistry 2025

Environ. Sci.: Nano, 2025, **12**, 3904–3920 | **3905**

To evaluate the influence of pH on the stability of NDs, the pH of NDs in NaCl suspensions with and without NOM was adjusted with NaOH solution.

The pH values were measured with a pH meter (Thermo Scientific™ Orion™ Versa Star Pro™). Prior to measurement, the pH meter was calibrated with standard buffer solutions with pH values of 4.0, 7.0 and 10.0. To investigate the stability of CDs and NDs under different conditions, the zeta potentials and particle size distributions were determined in model suspensions. The measurements were performed at time intervals of 0 h (zero time, measured directly after preparation of the suspensions), 4 h, 24 h, and 72 h.

2.3. Fourier-transform infrared spectroscopy

Dry samples of the investigated nanoparticles were analysed using FTIR spectroscopy. The samples were dried on a vacuum-assisted rotary evaporator, mixed with dry potassium bromide, and pressed into pastilles, which were then used for the analysis. The spectra were recorded in the wavelength range of 4000–500 cm^{-1} with a resolution of 4 cm^{-1} and 5 scans using a Spectrum Two FT-IR spectrometer (PerkinElmer) equipped with a deuterated triglycine sulfate (DTGS) detector.

2.4. Transmission electron microscopy

To assess the morphology and determine the primary size of CDs and NDs, a transmission electron microscope JEOL JEM-1400 Flash (JEOL, Tokyo, Japan) operated at 80 kV and equipped with a CMOS camera Xsarosa (EMSIS GmbH, Muenster, Germany) was used. For TEM analysis, a drop of suspension was placed on a copper grid covered with a hollow formvar membrane and the excess solution was removed with filter paper. Samples were dried in air and kept in a desiccator until analysis.

The primary size of the nanoparticles was determined using Image J v1.54g image analysis software (freely available at **https://imagej.net/ij/** (accessed on 4 December 2024)).

2.5. Dynamic and electrophoretic light scattering

The size distribution and zeta potential (ζ) of the prepared suspensions were determined by dynamic (DLS) and electrophoretic light scattering (ELS) using a Zetasizer Nano ZS (Malvern Instruments, Malvern, UK) equipped with a 532 nm "green" laser. To reduce multiple scattering and the effects of dust, the intensity of the scattered light was measured at a backscatter angle of 173°. To avoid overestimation due to the scattering of larger particles, the hydrodynamic diameter (d_h) was determined as the value at the peak maximum of the volume size distribution. Each sample was measured 10 times. The zeta potentials of the particles were calculated from the measured electrophoretic mobility with Henry's equation using the Smoluchowski approximation ($f(\kappa a) = 1.5$). The results are an average of 3 measurements. Zetasizer v6.32 software (Malvern

Instruments) was used for data processing. Both DLS and ELS measurements were performed at $\vartheta = 25$ °C.

2.6. Steady-state absorption measurements

For UV-vis measurements, samples were prepared by adding the required amount of nanoparticle suspensions in MQ water or NaCl to the BSA solution (5 μmol L^{-1}). Samples were incubated for 1 hour before measurements. The UV-vis spectra were recorded in the 800 nm to 250 nm range using an Agilent Cary 60 UV-vis spectrophotometer equipped with a Peltier 1 × 1 cell holder using quartz cuvettes with a 1 cm path length. The absorption titrations were performed at constant BSA concentration and varying concentrations of the nanomaterials (0, 30, 45, 60, 75, 90, and 105 mg L^{-1}). Measurements were performed in triplicate at 25 °C.

Calculation of the apparent association constant. Formation of the complex between BSA and nanomaterials (M) results in changes in BSA absorbance at 278 nm, which enables the determination of the apparent association constants K_{app} of the nanomaterials with BSA:[16,21,22]

$$\text{BSA} + \text{M} \overset{K_{app}}{\leftrightarrow} \text{BSA}\cdots\text{M} \quad K_{app} = \frac{[\text{BSA}\cdots\text{M}]}{[\text{BSA}][\text{M}]} \tag{1}$$

The Benesi and Hildebrand equation was used for calculating the values of K_{app} (Benesi *et al.*, 1949):

$$A_{obs} = (1 - \alpha)C_0\varepsilon_{BSA}l + \alpha C_0\varepsilon_c l \tag{2}$$

where A_{obs} is the absorbance of the BSA solution containing various concentrations of nanoparticles at 278 nm, α is the degree of association between BSA and nanoparticles, C_0 is the initial concentration of BSA, ε_{BSA} and ε_c are the molar extinction coefficients for BSA and the complex formed at 278 nm, respectively, and l is the length of the optical path. Eqn (2) can be modified to:

$$A_{obs} = (1 - \alpha)A_0 + \alpha A_c \tag{3}$$

where A_0 and A_c are the absorbance values of BSA and the complex at 278 nm, respectively. If the concentration of the material is relatively high, α can be considered equal to:

$$\alpha = \frac{K_{app}[\text{M}]}{1 + K_{app}[\text{M}]} \tag{4}$$

where $[\text{M}]$ is the concentration of the nanoparticles. Substituting eqn (4) into eqn (3) leads to the following expression:

$$\frac{1}{A_{obs} - A_0} = \frac{1}{A_c - A_0} + \frac{1}{K_{app}(A_c - A_0)[\text{M}]} \tag{5}$$

From the linear plot $\frac{1}{A_{obs} - A_0}$ *vs.* $\frac{1}{[\text{M}]}$ K_{app} can be determined from the slope and intercept.

3906 | *Environ. Sci.: Nano*, 2025, **12**, 3904–3920

This journal is © The Royal Society of Chemistry 2025

3. Results and discussion

3.1. FTIR analysis of carbon dots and nanodiamonds

The carbon dots CD1 and CD2 as well as the NDs were characterized using FTIR spectroscopy. Their spectra are shown in Fig. 1.

In the spectra of CD1 (Fig. 1a) and CD2 (Fig. 1b), a very broad absorption band with a maximum at approx. 3150 cm^{-1} is observed, which can be assigned to the O–H stretching vibrations of carboxyl groups. The O–H band of adsorbed water also appears in this region, usually at about 3450 cm^{-1}, and is often covered by a broad band of carboxylic acid (in the spectrum (a) it is visible at 3483 cm^{-1}). The stretching vibrations of the carbonyl groups (C=O) and the C=C bonds of the skeletal rings can be recognised in the CD1 spectrum as low intensity bands at 1697 and 1636 cm^{-1}, respectively. The band at 1399 cm^{-1} can be attributed to the bending vibrations of the C–H bonds, and the one at 1115 cm^{-1} to the stretching vibrations of the C–O bonds. Bands at 1599 cm^{-1} and 1403 cm^{-1}, observed in the CD2 spectrum but not in the CD1 spectrum, correspond to the asymmetric and symmetric stretching vibrations of the carboxylate anions (COO$^-$), respectively.[23]

On the other hand, in the spectrum of NDs (Fig. 1c), in addition to the broad absorption band of O–H groups at 3424 cm^{-1} (which may originate from carboxyl groups and adsorbed water[23]), as well as the low-intensity band of stretching vibrations of C=O carboxyl groups at 1742 cm^{-1}, the bands of the asymmetric and symmetric stretching
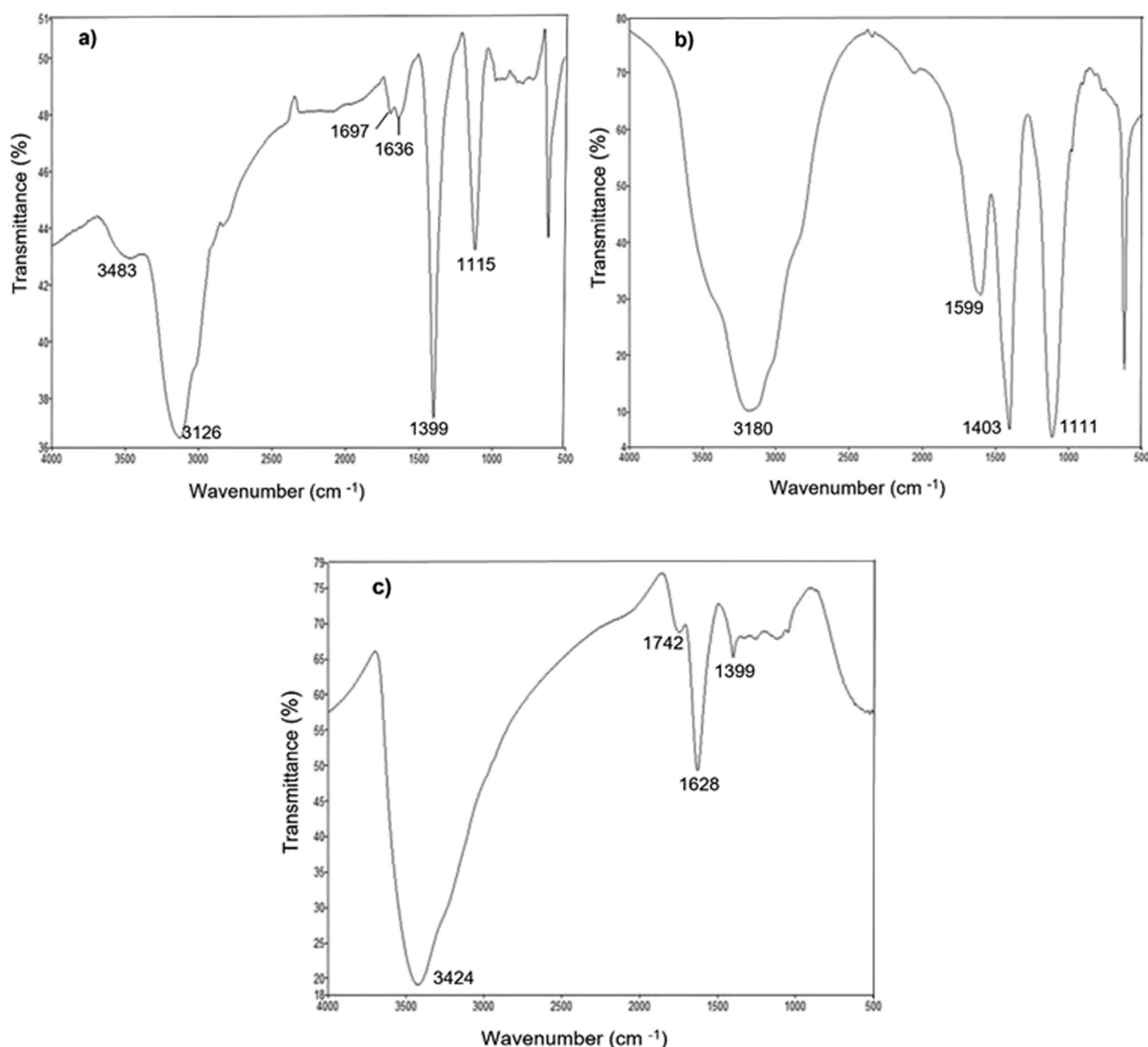

Fig. 1   FTIR spectra of carbon dots (a) CD1 and (b) CD2 and nanodiamonds (c) NDs.

vibrations of carboxylate anions (COO^-) at 1628 and 1399 cm^{-1}, respectively, can also be observed.

3.2. TEM characterization of carbon dots and nanodiamonds

The TEM images of the investigated nanoparticles are shown in Fig. 2. Both carbon dots were spherical and had an average size of 14.4 ± 6.8 nm and 6.9 ± 1.3 nm for CD1 and CD2, respectively. In both cases, small spherical particles were observed embedded in the matrix, probably originating from the remaining reactants. In contrast, the ND sample consisted of individual small spherical particles (Fig. 2c) with an average size of 17.5 ± 5.2 nm.

3.3. Stability of carbon dots and nanodiamonds in model suspensions

Two different model systems of carbon-based nanoparticles were investigated in terms of their stability in both water and aqueous NaCl solution, mimicking their behaviour in a river environment. The first model system involved suspensions of CDs in water and an aqueous NaCl solution, while the second one involved suspensions of NDs in water and an aqueous NaCl solution.

Fig. 3 shows the volume size distribution of CD particles in water (Fig. 3a and c) and aqueous NaCl solution (Fig. 3b and d) at intervals of 0 h, 4 h, 24 h, and 72 h. It can be seen from the figure that the volume size distributions of
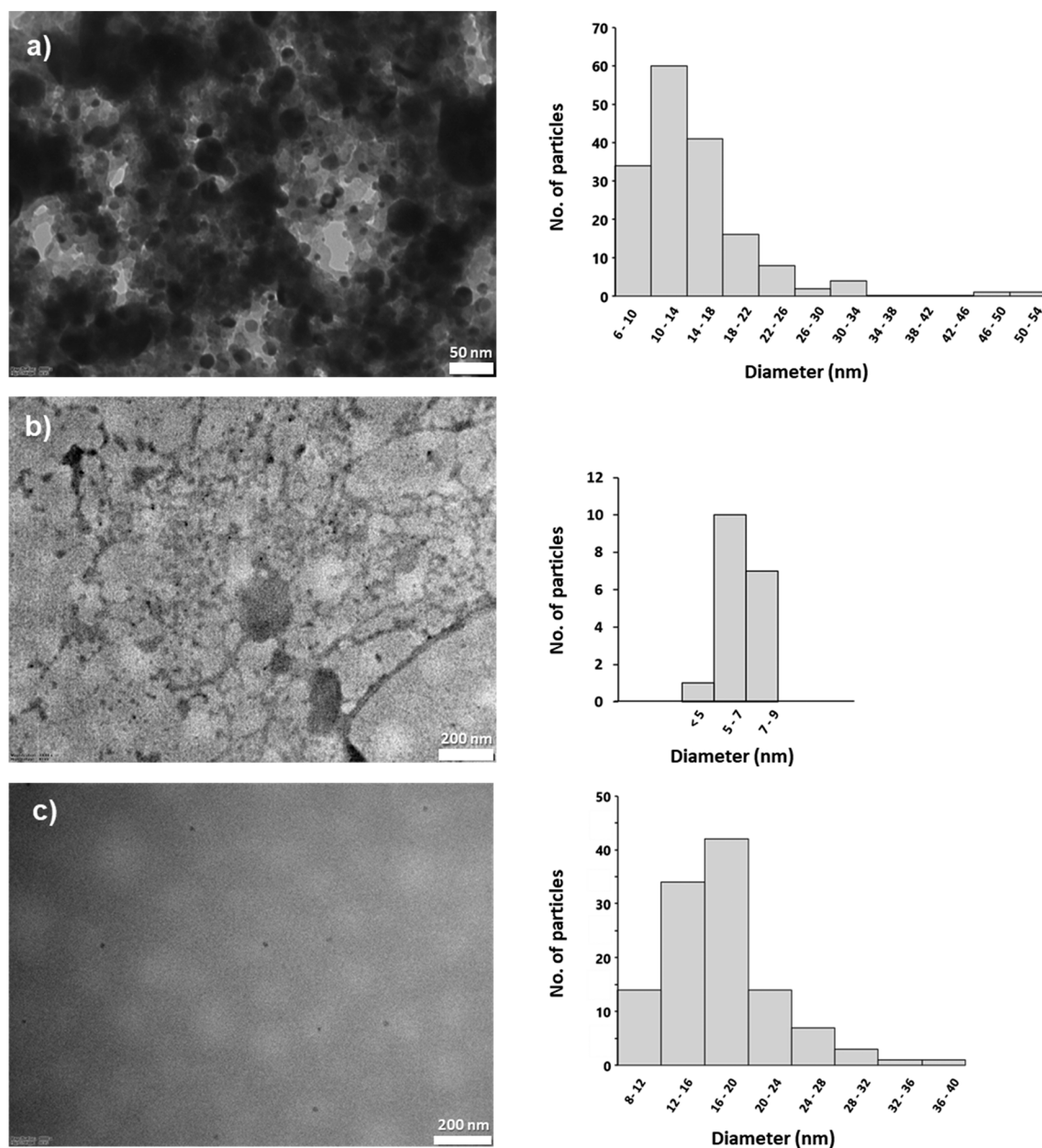

Fig. 2 TEM images and corresponding size distribution histograms of carbon dots (a) CD1 and (b) CD2, and (c) nanodiamonds NDs.
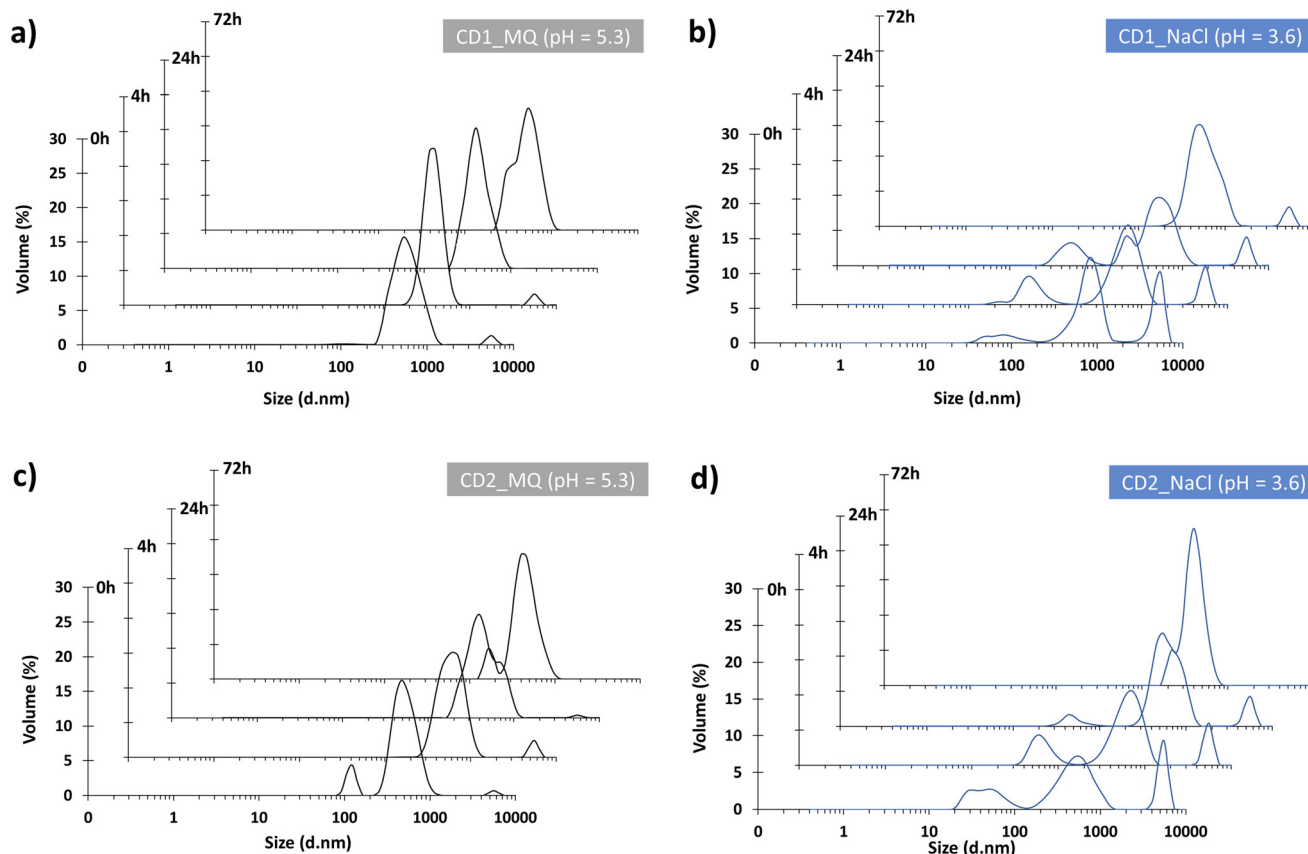
3908 | Environ. Sci.: Nano, 2025, 12, 3904–3920

This journal is © The Royal Society of Chemistry 2025

Fig. 3 Volume distribution of CD particle size in MQ water (a and c) and aqueous NaCl solution (b and d) after 0 h, 4 h, 24 h, and 72 h.

both CD samples in MQ water (left) differ significantly from those in NaCl solution (right), with significant shifts in peak positions and vol%. The dominant populations of CD1 and CD2 particles were found in both media in the size range of 400–800 nm. The somewhat narrower distribution in MQ water (pH 5.3) changed to a trimodal distribution in NaCl suspensions (pH 3.6), indicating the formation of aggregates of different sizes. The shift in the peak of the dominant population towards larger sizes (from 400–500 nm to 700–800

nm in the first 4 h) and an increase in the volume percentage of the population of the largest particles indicate that aggregation occurs to a greater extent in NaCl than in MQ water. The addition of NaCl probably reduced the electrostatic repulsion between the particles and thus promoted aggregation.[24–26]

In addition, the lower pH in the NaCl solution could cause some components of the particles to dissolve or be chemically transformed, possibly releasing smaller particles
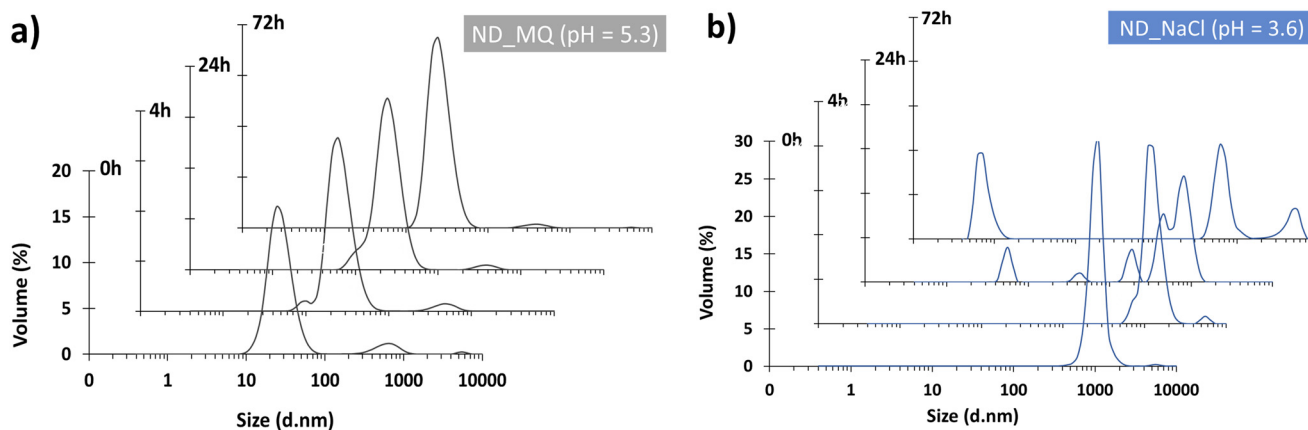

Fig. 4 Volume distribution of ND particle size in MQ water (a) and aqueous NaCl solution (b) after 0 h, 4 h, 24 h, and 72 h.

This journal is © The Royal Society of Chemistry 2025

Environ. Sci.: Nano, 2025, **12**, 3904–3920 | **3909**

or ions that interact with each other or with NaCl to form new aggregates, which can be observed as an appearance of a peak at sizes of 100 nm and smaller. After 72 h, this smallest population of particles is no longer detectable.

Contrary to CDs, NDs showed somewhat different behaviour. Fig. 4 shows the volume size distribution of ND particles in water (Fig. 4a) and aqueous NaCl solution (Fig. 4b) at intervals of 0 h, 4 h, 24 h, and 72 h. In MQ water (pH 5.3), a dominant peak at about 24 nm was observed, which, based on the value of primary size determined by TEM, probably corresponded to single ND particles. In addition, a population of larger particles, with an average size of about 400 nm, was also observed. The low intensity of these peaks likely represents less stable, transient aggregates that form sporadically between ND particles in water. However, their relatively low intensity indicates that aggregation is not prevalent in this medium.

In contrast, in the NaCl suspension (pH 3.6), the number of particle populations of different sizes increased with time, indicating considerable heterogeneity in the particle size distribution. This could indicate that the presence of NaCl destabilizes the system and promotes the formation of different ND aggregates. The size distributions obtained at different intervals indicate continuous particle aggregation, where aggregates form over a range of sizes without

stabilizing at a particular size. This results in a complex system, reflecting the unstable and dynamic nature of the system.

To get more detailed insight into the behaviour of investigated nanoparticles, the change in the zeta potential of the CDs and NDs in investigated media was determined (Fig. 5). As expected in all cases, the ζ potential values were less negative in the NaCl solution due to the screening of electrostatic interactions.[27,28]

As can be seen from Fig. 5, the ζ potential values of CDs in water during 72 h ranged from −28.3 mV to −21.4 mV for CD1 (Fig. 5a) and from −34.8 mV to −20.2 mV for CD2 (Fig. 5b), whereas for the model suspension of CDs in aqueous NaCl solution, the ζ potential values ranged from −17.6 mV to −12.8 mV for CD1 (Fig. 5a) and from −18.6 mV to −14.0 mV for CD2 (Fig. 5b). While the zeta potential of the CDs was more negative in MQ water than in NaCl solution, confirming greater stability in the former, the lack of a clearly defined trend over time also suggests that stability, although it can be maintained over short periods of time, may be affected by factors other than electrostatic interactions.

The ζ potential values of the model suspension of NDs in water, on the other hand, ranged from −54.3 mV to −44.5 mV and showed a slight decrease over time, whereas the ζ potential values of the ND suspension in aqueous NaCl
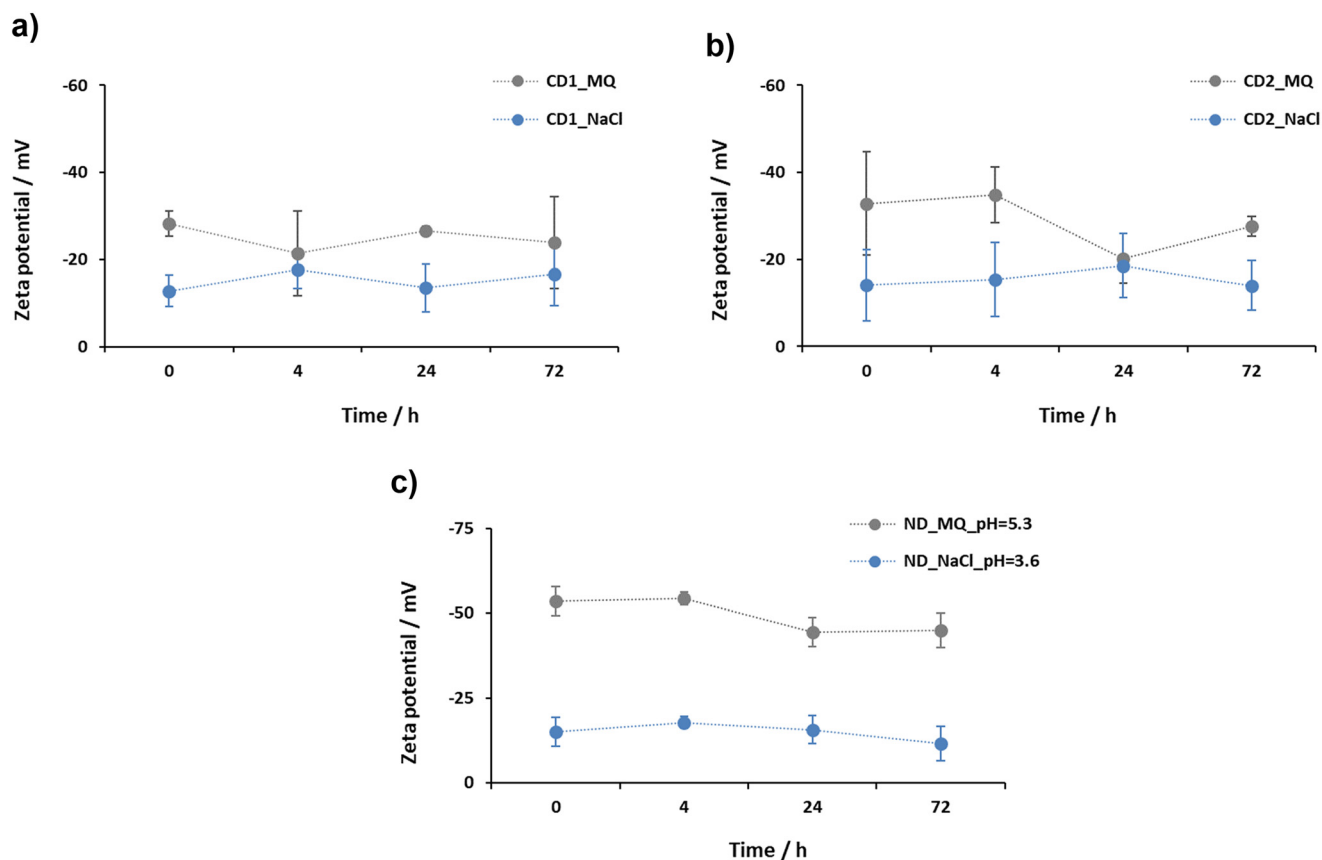

Fig. 5 Change in zeta potential over time for CD (a and b) and ND (c) suspensions in water (MQ) and aqueous NaCl solution. Data are shown as the mean ± standard deviation (n = 3).

3910 | *Environ. Sci.: Nano*, 2025, **12**, 3904–3920

This journal is © The Royal Society of Chemistry 2025

solution ranged from −17.8 mV to −11.5 mV and were characterized by a slight increase in the first 4 h followed by a slight decrease in the remaining time (Fig. 5c). The much larger difference in the ζ potential of NDs in the two investigated media, compared to CDs, indicates the more expressed importance of electrostatic interactions for the stability of NDs than for CDs and explains the difference in behaviour observed by DLS measurements (Fig. 3 and 4).

The behavior of nanoparticles in water solution is governed by various factors, including their surface chemistry, size, shape, and charge.[5] The lower zeta potential of CDs and their tendency to form agglomerates in MQ water (under acidic conditions) in contrast to the stability of NDs can be linked to differences in their surface chemistry, as revealed by the FTIR spectra (Fig. 1). Namely, both types of carbon dots exhibit abundant surface functional groups, including hydroxyl (O–H), carbonyl (C=O), and carboxyl (COOH) groups, as indicated by the broad absorption bands in the 3150–3480 cm^{-1} region, low intensity band at 1697 cm^{-1} and distinct carboxylate peaks at 1599 and 1403 cm^{-1} (particularly in CD2). Under acidic conditions, protonation of these functional groups, especially the carboxyl and hydroxyl moieties, reduces the surface charge and weakens electrostatic repulsion between particles. This charge neutralization promotes aggregation, leading to reduced colloidal stability of carbon dots in low pH environments. Also, these polar groups can interact with water molecules through hydrogen bonds,[29] which leads to a reduction in the effective charge and lower stability of the particles in suspension. All of the above is reflected in the volume size distribution of CD1 and CD2 and the predominance of particles with a diameter of over 100 nm (Fig. 3). Since the detected particles are larger compared to their primary size determined by TEM, this indicates their low stability in water. The slightly better stability of CD2 in water compared to CD1 (Fig. 5a and b) can be explained by the presence of carboxylate anions in addition to the hydroxyl, carboxyl, and carbonyl groups, as shown in the FTIR spectra (Fig. 1a and b).

In contrast to CD1 and CD2, the FTIR spectrum of NDs (Fig. 1c) shows a narrower O–H band at 3424 cm^{-1} and well-resolved carboxylate bands at 1628 and 1399 cm^{-1}, indicating the presence of more stable, deprotonated surface groups. The weaker intensity of the C=O stretching band at 1742 cm^{-1} suggests a lower density of protonatable carboxylic acids compared to the carbon dots. As a result, NDs maintain a higher surface charge and better colloidal stability in acidic environments. This observation is in accordance with previous modelling[30] and experimental studies.[10,31] Additionally, carboxylated NDs may also have nonpolar groups on their surface that can interact with water molecules through hydrophobic interactions,[32] further contributing to their higher stability in water compared to CDs. The stability of NDs in water is also evidenced by their consistent particle size distribution over time (Fig. 4a) with an average size of the dominant population of particles (~24

nm) smaller than in the case of CDs (varying between 400 nm and 500 nm), unlike in NaCl suspensions where the salt presence screens the electrostatic interactions between ND particles, causing them to enlarge and initially aggregate (Fig. 4b). From 24 h to 72 h, a shift towards smaller particle sizes suggests extensive aggregation, sedimentation, and subsequent removal from the suspension.

3.4. Influence of the additives on ND stability

Due to their overall lower stability in water, CDs were excluded from further experiments. In subsequent experiments, NDs were selected to explore their interactions with various substances that are naturally present in the environment, such as proteins (BSA), pollutants (DSS), and organic matter (FA and NOM). This approach was aimed at understanding how NDs behave under real-world conditions and interact with components commonly found in natural ecosystems.

Due to limited sample sizes, the pH values of BSA suspensions were estimated from the literature to be between 3 and 4. DSS showed pH values of 5.5 in water and 4 in NaCl solution, while FA had pH values of 4.1 in water and 3.1 in NaCl solution. The pH of NOM was 5.0 in water and 3.2 in NaCl solution.

Prior to the addition to ND suspensions, the volume distribution of particle size of all additives in both water and aqueous NaCl solution, at 0 h, was determined (Fig. 6). DLS measurements of the BSA suspension in water and NaCl solution revealed a uniform particle size distribution, with a dominant population averaging ~4.5 nm and ~5.7 nm, respectively. In contrast, the DSS distribution in water showed a dominant population averaging ~70 nm, which, in the aqueous NaCl solution, changed to bimodal distribution with a dominant particle population having a size of ~25 nm (88.5 vol%) and a small amount (11.5 vol%) of larger particles with a size of ~60 nm. Fulvic acid showed a monomodal distribution of particle size averaging ~120 nm in water and ~130 nm in NaCl solution, while natural organic matter exhibited a particle population with size averaging ~150 nm in water and ~133 nm in NaCl solution.

Fig. 7 shows the volume distribution of the particle size of ND and BSA suspensions in water and aqueous NaCl solution, respectively, at the time intervals of 0 h, 4 h, 24 h, and 72 h. While DLS measurements of the ND and BSA suspension in water (pH ~3–4) revealed a uniform particle size distribution over time, with a dominant population averaging ~24 nm, the distribution in aqueous NaCl solution (pH ~3–4; Fig. 7b) shifted significantly, indicating instability of the suspension under these conditions. During the initial 4 h, the detection of particles ranging from 1000 nm to 6500 nm suggests significant aggregation. After 24 h and 72 h, smaller particles (~6.5 nm) predominated, indicating the sedimentation of larger aggregates and the existence of individual BSA particles. These findings are consistent with our observations for BSA in NaCl (with a dominant

This journal is © The Royal Society of Chemistry 2025

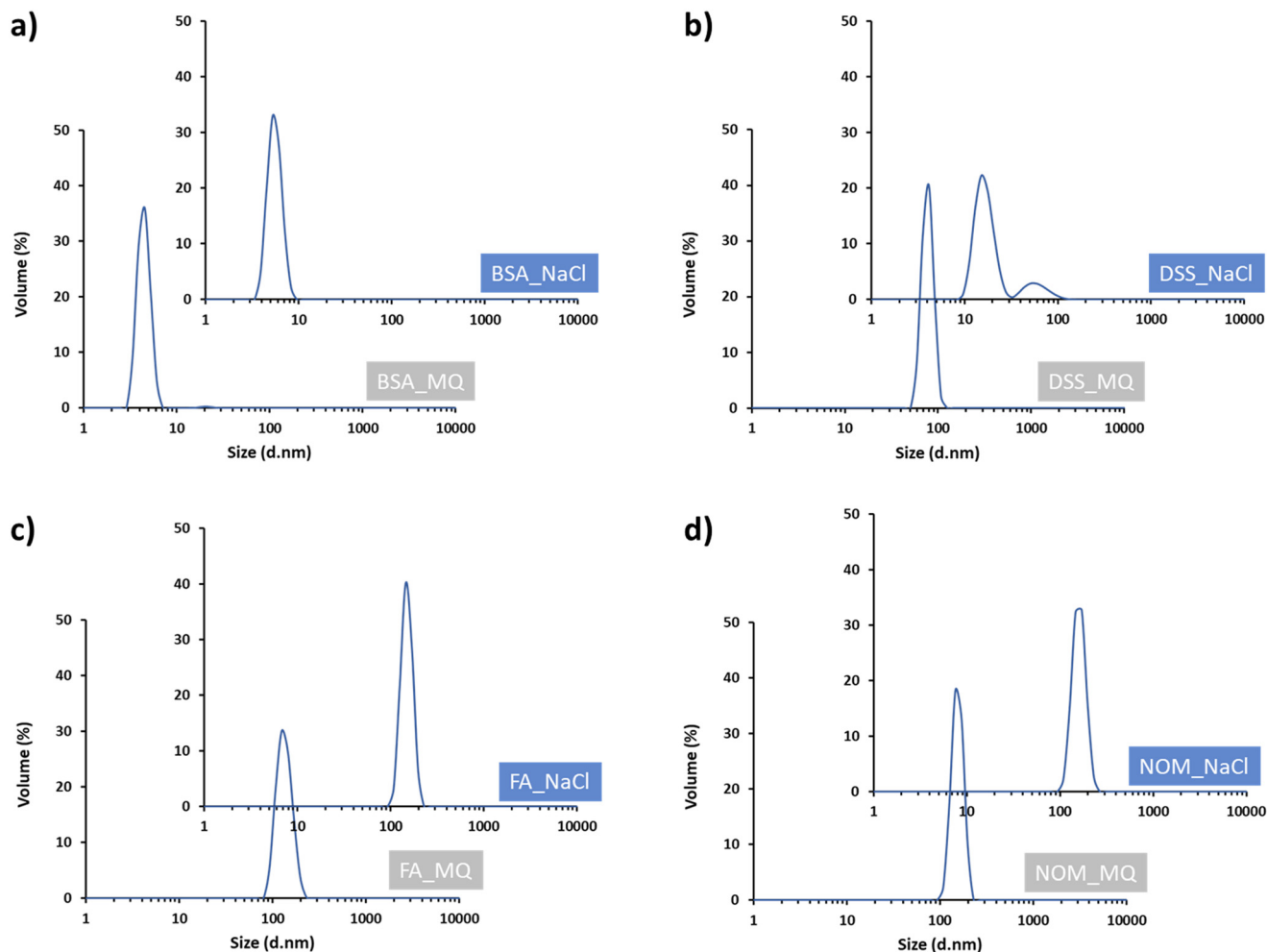Environ. Sci.: Nano, 2025, 12, 3904–3920 | 3911

Fig. 6 Volume distribution of particle size in MQ water and aqueous NaCl solution at 0 h for BSA (a), DSS (b), FA (c), and NOM (d).

population averaging ~5.3 nm; Fig. 7a) and corroborate previously reported sizes, such as ~7.1 nm (ref. 33) and 6.8 ± 0.1 nm under pH 3 and 150 mM NaCl conditions.[34] However, our findings differ to some extent from those of Kulvelis *et al.*,[35] who reported stability of water and saline ND suspensions in the presence of BSA. The stabilization method for detonation NDs in saline media, proposed by these authors, presents a solution for biomedical applications that require a PSU of about 0.9 to mimic physiological environments such as blood plasma. In contrast, the NaCl concentration of 15 mg L^{-1} used in this study more closely resembles riverine conditions rather than a physiological environment. Specifically, this concentration corresponds to a salinity of about 0.015 PSU, which falls within the range defined for freshwater systems (*i.e.* salinity < 0.5 PSU).[36]

Fig. 8a shows the change in the zeta potential of a suspension of NDs in water and aqueous NaCl solution with the addition of BSA. Since the zeta potential of the ND particles in water with (ζ from −22.2 mV to −16.0 mV; Fig. 8a) and without (ζ from −54.3 mV to −44.5 mV; Fig. 4a) BSA differed significantly, it can be assumed that adsorption of

BSA occurred at the surface of the ND particles.[7] The difference in zeta potential between ND particles in an aqueous NaCl solution with and without BSA was, however, small (ζ from −17.6 mV to −11.0 mV with BSA, ζ from −17.8 mV to −11.5 mV without BSA), suggesting that in the presence of NaCl, the chemical interactions between BSA and the ND surface may be altered or disrupted, leading to reduced stability of the suspension and potential aggregation of particles over time. This is consistent with DLS measurements (Fig. 7b) as well as previous studies on the adsorption of proteins on NDs and the effects of suspension composition on protein adsorption.[6,37,38] Namely, the adsorption behavior of proteins on nanoparticles and their overall stability is influenced by various factors, including the size, surface chemistry, and charge of the nanoparticles, as well as the properties of the protein and the surrounding solution.

Despite the decrease of zeta potential in the suspension of NDs and BSA in water with time, it is evident from Fig. 7a that the size of the particles does not change, *i.e.*, it remains at around ~24 nm, from which it can be concluded that the particles remain dispersed. This is in
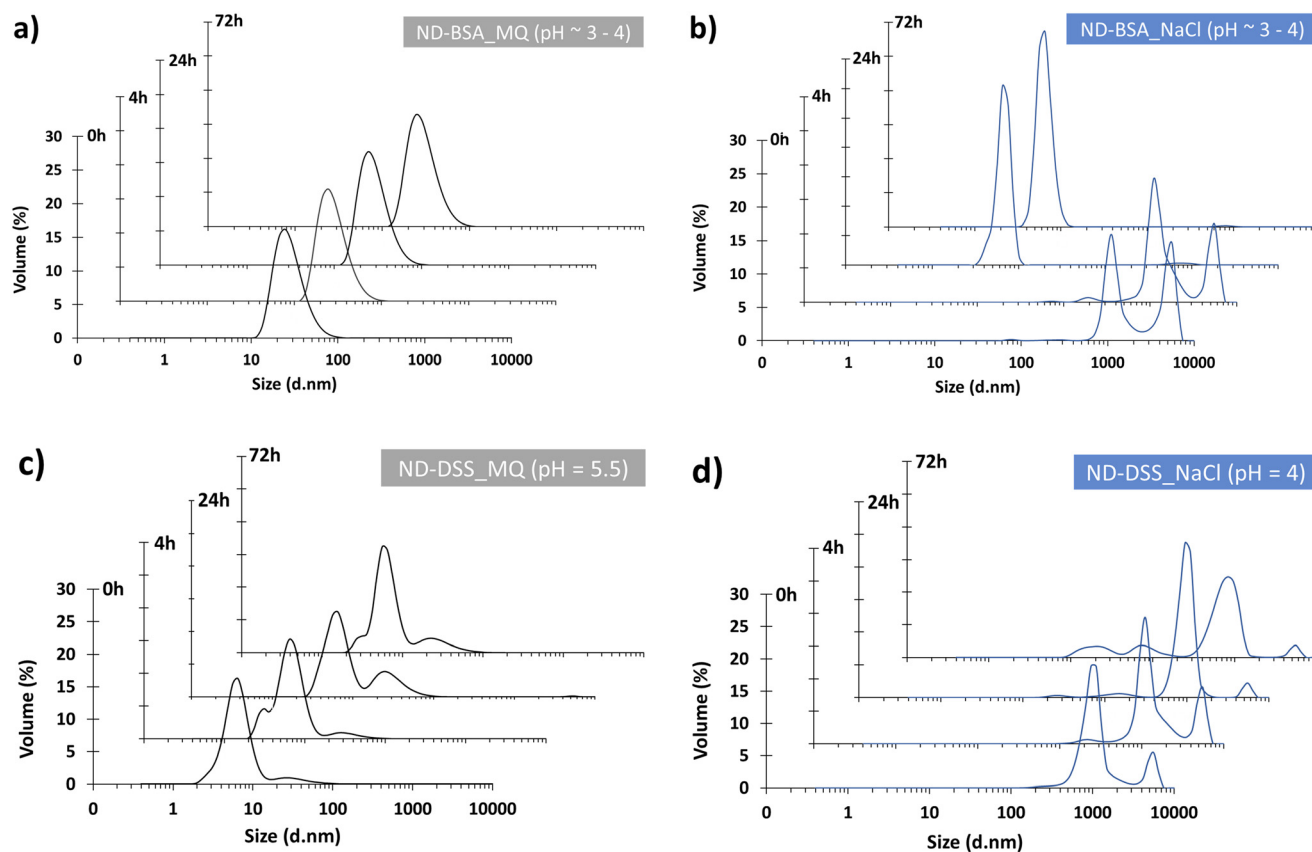
Fig. 7 Volume distribution of particle size of NDs and BSA and DSS in MQ water (a and c) and aqueous NaCl solution (b and d) after 0 h, 4 h, 24 h, and 72 h.

accordance with the literature, which mentions the positive effect of BSA on the stabilization of the suspension[12] due to steric shielding.

Fig. 7 also shows the volume distribution of the particle size of ND and DSS suspensions in water (pH = 5.5; Fig. 7c) and in aqueous NaCl solution (pH = 4; Fig. 7d) over time, *i.e.* after 0 h, 4 h, 24 h and 72 h. Compared to the model suspension of NDs in water (Fig. 4a), the observed reduction in particle size in the presence of DSS (with a dominant population averaging 6.5 nm over time; Fig. 7c) indicates enhanced electrostatic repulsion, suggesting dispersed particles. This phenomenon can be attributed to the presence of carboxyl functional groups on the surface of the NDs, which facilitate repulsion between negatively charged units. DSS, being a polyanion, further contributes to electrostatic repulsion thereby promoting dispersion. Porsch and Sundelöf[39] demonstrated that dextrans in aqueous suspensions do not form aggregates, with detected particle sizes ranging from 110 to 170 nm. Similarly, Madkhali *et al.*[40] reported that in an injectable colloidal system, DSS nanoparticles exhibited a maximum particle size of 69.3 nm, with the particle size distribution (radius) ranging from 52 to 82 nm. Our measurements corroborated these findings, with DSS in MQ water exhibiting a dominant particle size averaging ~70 nm (Fig. 6b). Conversely, an increase in particle size is observed in a NaCl solution spiked with DSS

(with a dominant population averaging from 825 to 1100 nm over time) (Fig. 7d), indicating the formation of aggregates.

For ND and DSS suspensions in both water and aqueous NaCl solution (Fig. 8b), large negative values of zeta potential were obtained, ranging from −56.0 mV to −46.9 mV in water and from −42.3 mV to −27.7 mV in NaCl solution, suggesting stability of both suspensions. This indicates that the aggregation of NDs in the presence of DSS in NaCl observed by DLS is not a consequence of electrostatic interaction. A possible explanation could be the bridging of the ND particles by DSS.

Dextran sulfate sodium (DSS) is a synthetic compound widely used in biomedical research, especially in animal models of colitis and inflammatory bowel disease to induce intestinal inflammation.[17] It is worth noting that dextran, a polysaccharide analogous to DSS, is naturally occurring and can be found in various environmental niches, including microbial biofilms, soil, and aquatic ecosystems.[41,42] These naturally occurring dextran polysaccharides play diverse roles in microbial physiology and interactions with the environment. Despite the ionic nature of DSS, which makes it more water-soluble than dextran, its presence can significantly influence interactions with other aqueous substances, such as proteins or nanoparticles. Therefore, DSS can serve as a model representative for other negatively charged polysaccharides commonly found in aqueous
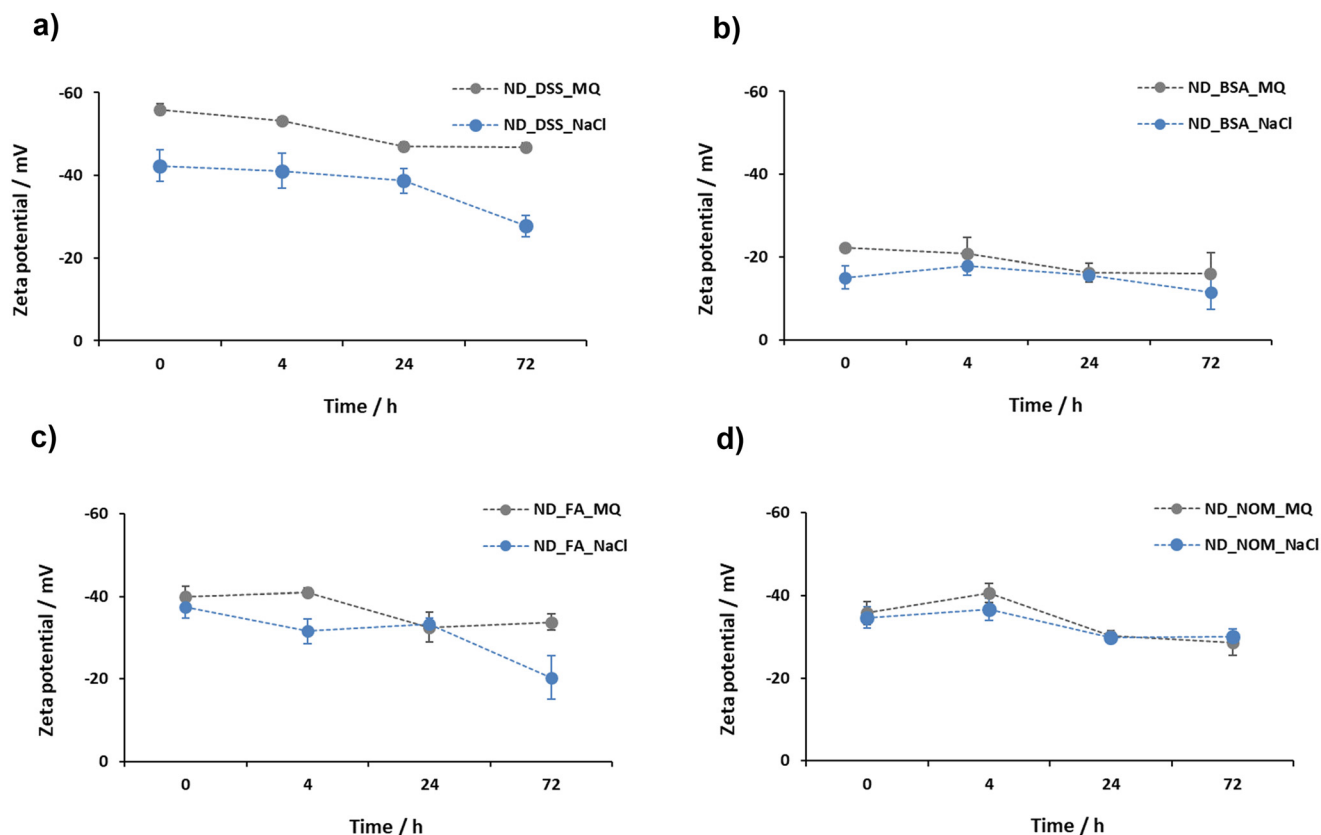
This journal is © The Royal Society of Chemistry 2025

Environ. Sci.: Nano, 2025, **12**, 3904–3920 | **3913**

Fig. 8 Change in zeta potential over time for NDs in water and aqueous NaCl solution with addition of DSS (a), BSA (b), FA (c), and NOM (d). Data are shown as the mean ± standard deviation (n = 3).

environments, including hyaluronic acid, pectin, and alginates. However, a detailed comparison with the existing literature is unattainable, as to our knowledge, this study presents the first dataset on the behavior of NDs and DSS in model aqueous suspensions.

Fig. 9 shows the volume size distribution of ND suspensions in water (pH = 4.1; Fig. 9a) and aqueous NaCl solution (pH = 3.1; Fig. 9b) containing FA, respectively, at the time intervals of 0 h, 4 h, 24 h, and 72 h. In the former, a uniform distribution of particle size (with a dominant population averaging 32 nm over time) over the 72 h period can be observed. However, in the latter case (*i.e.* in aqueous NaCl solution), the observed increase in particle size (with a dominant population averaging 955 nm over time) indicates the formation of aggregates in addition to the presence of smaller particles in the NaCl suspension.

The behavior of the suspension of NDs and NOM shows different properties than the suspension of NDs and FA. Namely, Fig. 9 shows the volume distribution of the particle size for the ND and NOM suspensions in water (pH = 5.0; Fig. 9c) and aqueous NaCl solution (pH = 3.2; Fig. 9d) at different time intervals. The results show a slight shift to the larger sizes in the water medium (Fig. 9c), indicating a slight increase in particle size (with a dominant population averaging 48 nm over time). Conversely, a broader particle size distribution and a higher proportion of larger particles

can be seen in the presence of NaCl (Fig. 9d) compared to water (Fig. 9c).

In the presence of FA and NOM, the particle size distribution of NDs in aqueous suspension shows remarkable changes compared to their individual behavior in water (Fig. 6c and d), while remaining relatively stable over time. In particular, the dominant population in the combined system, *i.e.* NDs and FA (32 nm) or NDs and NOM (48 nm), is larger than that observed for NDs alone (24 nm), but smaller than the sizes observed for FA (125 nm) or NOM (146 nm) individually. This behavior indicates that FA and NOM weakly stabilize NDs through interactions that are insufficient to prevent aggregation under high-ionic-strength conditions.

The zeta potential values presented in Fig. 8c show a decrease in the absolute value for the ND water suspension after the addition of FA, from −45.0 mV to −33.8 mV. Despite this decrease, which indicates a reduction in colloidal stability, the zeta potential remains in the range typically associated with stable suspensions. This decrease is consistent with previous research showing a decrease in colloidal stability following the introduction of certain organic molecules.[43] The minimal changes in particle size over time observed in Fig. 9a emphasize, however, the continued stability of the suspension, regardless of the decrease in zeta potential.
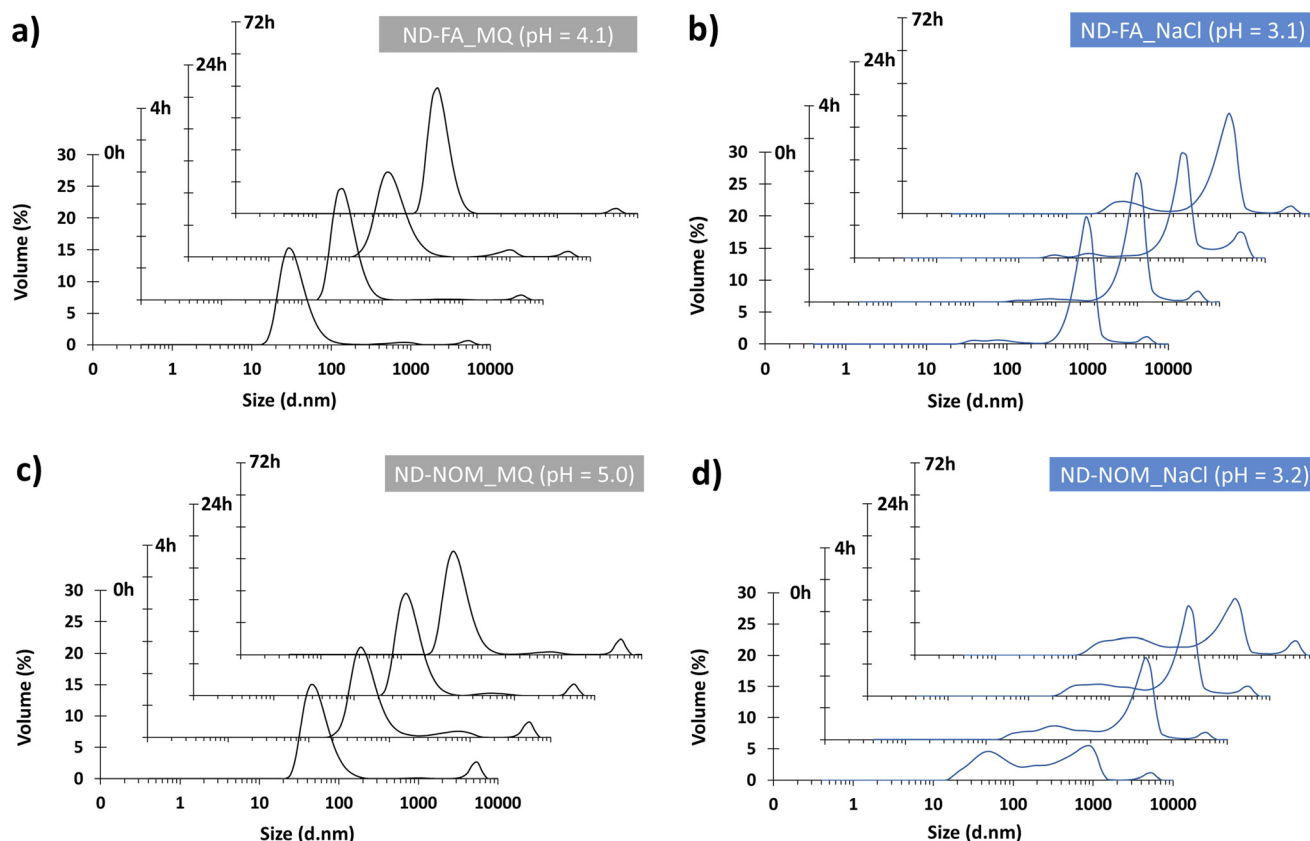
Fig. 9 Volume distribution of particle size of NDs and FA and NOM in MQ water (a and c) and aqueous NaCl solution (b and d) after 0 h, 4 h, 24 h, and 72 h.

In contrast, in the aqueous NaCl solution containing NDs and FA (see Fig. 8c), an increase in absolute zeta potential can be observed compared to the measurement of NDs without additives (Fig. 5c). However, the final value reached after 72 h (ζ = −20.3) indicates certain instability of the suspension in the aqueous NaCl solution. This is corroborated by an increase in particle size (Fig. 9b), which can be attributed to the formation of aggregates.

The results of the ND suspensions with the addition of FA and NOM differ from those in the literature, particularly in terms of surface charge and zeta potential. Previous studies described ND suspensions characterized by a positively charged surface and a positive zeta potential,[44] while our observations indicate the opposite: a negative zeta potential and a negatively charged surface, which is due to functionalization with –COOH groups. Chernysheva et al.[44] documented that interactions between humic substances and nanodiamonds produced by detonation led to a reversal of the zeta potential from positive to negative values. While ND–humic acid suspensions exhibited zeta potential values typically associated with stable nanoparticles, ND–FA suspensions showed lower zeta potential values, indicating lower colloidal stability, which had a positive effect on ND uptake by wheat seedlings compared to HA.[44]

In summary, the addition of BSA elicited the most notable reduction in absolute zeta potential in water, primarily due to the adsorption of the protein on the ND surface. FA and NOM showed a similar effect, reducing the absolute zeta potential value while maintaining the stability of the suspension in the ND matrix. Conversely, the addition of DSS had the least impact on the zeta potential, likely due to heightened electrostatic repulsion between the negatively charged ND and DSS units, resulting in highly stable particles in suspension compared to other additives.

In the context of aqueous NaCl solution, all additives, except BSA, increased the absolute zeta potential value compared to ND suspensions without additives. It is noteworthy that the particle size distribution in all suspensions remained stable over a period of 72 h in water, indicating a dispersed particle state. Conversely, suspensions with DSS, FA and NOM additives in aqueous NaCl solution exhibited stable particle size distributions over the same time period but showed aggregates with an average size of about 1000 nm. Remarkably, suspensions of NDs and NDs with BSA in aqueous NaCl solution showed temporal instability characterized by significant variations in the size distribution within the first 24-hour interval, indicating intense aggregation and rapid sedimentation of the aggregated units.
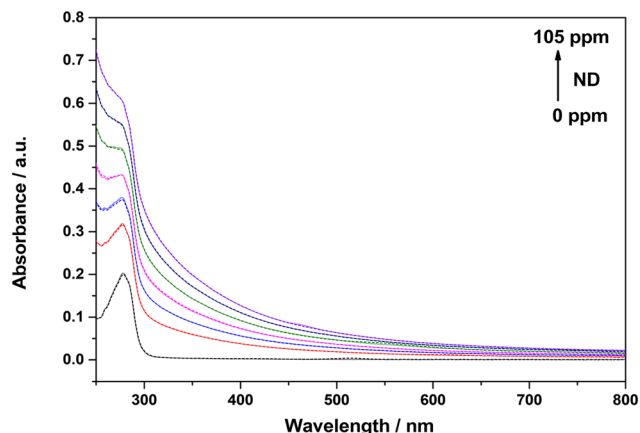
Fig. 10 UV-visible absorption spectra (from bottom to top) of BSA (c(BSA) = 5 μmol dm^{-1}) and BSA in the presence of 30 mg dm^{-3}, 45 mg dm^{-3}, 60 mg dm^{-3}, 75 mg dm^{-3}, 90 mg dm^{-3}, and 105 mg dm^{-3} NDs at 25 °C.

3.5. Spectroscopic studies of the interactions between BSA and NDs

To gain a better insight into the BSA interactions with NDs, equilibrium properties were investigated. This allowed an evaluation of the strength of BSA binding in different media.

UV-vis spectroscopy is often used to study protein interactions with nanoparticles, as the increase in protein absorbance due to the presence of NPs provides information about specific molecular interactions.[45] The absorbance spectra of pristine BSA and BSA in the presence of NDs at different concentrations are shown in Fig. 10.

In the UV-vis spectra (Fig. 10), a gradual increase in BSA absorbance at 278 nm was observed with increasing concentration of the NDs, which can be attributed to the formation of complexes between BSA and NDs[16,21,22,46] confirming the zeta-potential results. No shift in the position of the absorption maximum was observed in the presence of the NDs, which could indicate that no

significant conformational changes in the BSA structure occurred.[37]

To compare the binding strength of NDs, the K_{app} was calculated using eqn (5).

The K_{app} value of 1.207 ± 0.067 mol^{-1} dm^3 was obtained for interaction in MQ while 1.184 ± 0.001 mol^{-1} dm^3 for interaction in NaCl. It can be concluded that there is no significant change in the binding strength of the NDs in these two media. This points to the possibility that in freshwater environments, BSA will remain adsorbed on the NDs. To the best of our knowledge, no similar study has been conducted under the model environmental conditions.

3.6. Variation of the pH of the suspensions

Since pH can have an effect on zeta potential values, its influence on the stability of ND suspensions in aqueous NaCl solution, both with and without natural organic matter (NOM), was investigated. Particle size distribution analysis for NDs in NaCl solution at pH 10 showed initial particle size reduction, compared to the same suspension at pH 3.6, followed by aggregation after 24 h (Fig. 11a). Meanwhile, ND–NOM suspensions remained stable over time with a dominant population averaging ~24 nm (Fig. 11b), indicating efficient dispersion.

The zeta potential variations over time for ND suspensions at pH 10 and 3.6, and ND–NOM suspensions at pH 9 and 3.2, are depicted in Fig. 12. While differences between pH 9 and 10 might be expected due to pH alone, regardless of the influence of NOM, the comparison remains environmentally relevant, as such a variation is relatively minor within the alkaline range commonly encountered in natural systems.

The obtained data revealed that ND suspensions in aqueous NaCl solution exhibit greater stability at higher pH levels (alkaline range), with zeta potential values of around −30 mV at pH 10, indicative of moderate stability, compared to −15 mV at pH 3.6. This stability increase is attributed to the deprotonation of carboxyl (–COOH) groups on the ND
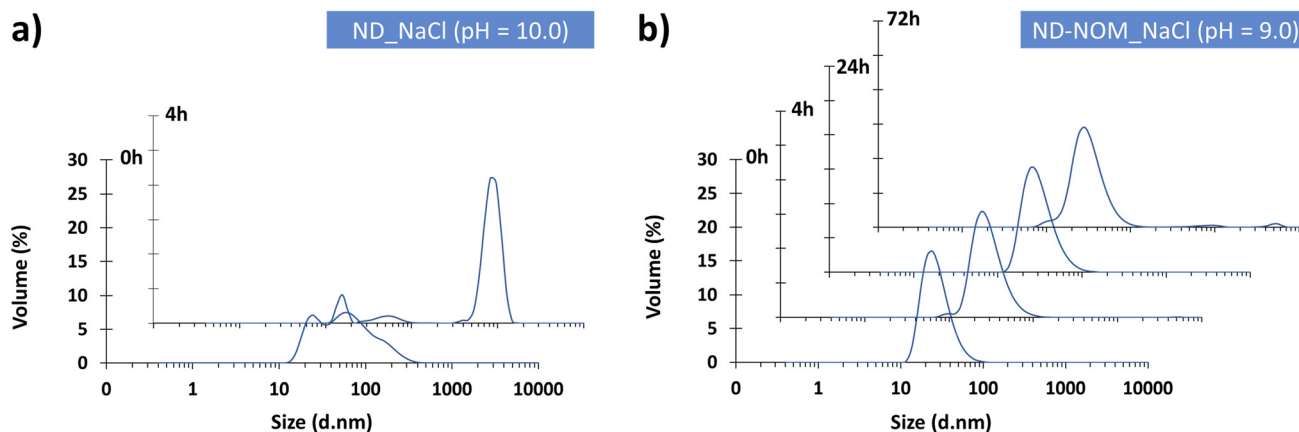

Fig. 11 Volume distribution of particle size of (a) NDs in aqueous NaCl solution, at pH = 10, obtained after 0 h and 24 h, and (b) ND and NOM suspension in aqueous NaCl solution, at pH = 9, obtained after 0 h, 4 h, 24 h and 72 h.
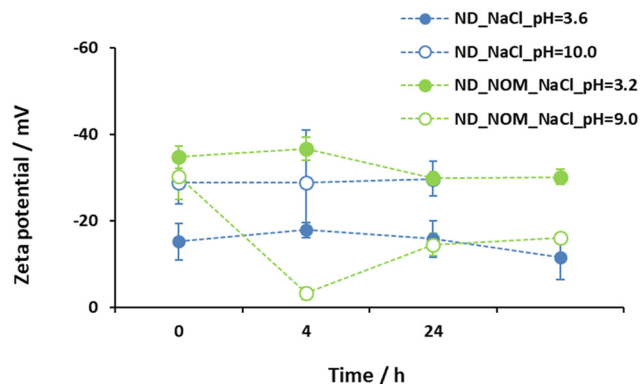
3916 | Environ. Sci.: Nano, 2025, **12**, 3904–3920

This journal is © The Royal Society of Chemistry 2025

Fig. 12 Change in zeta potential over time for NDs in aqueous NaCl solution at different pH values and in the presence or absence of NOM. Data are shown as the mean ± standard deviation (n = 3).

surface under alkaline conditions, resulting in negatively charged carboxylate groups (–COO⁻).[47] The resulting surface charge enhances electrostatic repulsion and dispersion.[8] In contrast, under acidic conditions, the carboxyl groups remain protonated,[47] leading to a less negative or neutral surface charge, reduced repulsion, and increased particle aggregation.

Conversely, ND–NOM suspensions showed a trend of increased ζ potential values at lower pH levels (acidic range) with ζ ranging from −34.7 mV to −29.8 mV, compared to a notable rise in zeta potential from −30.2 mV to −3.13 mV after 4 h, then decreasing to −16.0 mV after 72 h under alkaline conditions. Despite this, DLS results showed that ND–NOM suspensions in NaCl are rather stable under alkaline conditions (Fig. 11c) compared to acidic conditions (Fig. 9d).

While NDs in aqueous NaCl solution exhibit increased stability in an alkaline environment, this behavior is primarily driven by enhanced electrostatic repulsion promoted by the electrically charged carboxyl groups on their surfaces. At a higher pH, the carboxyl groups on the ND surface are deprotonated, resulting in a stronger negative surface charge and a more negative zeta potential (Fig. 12). In contrast, under acidic conditions, these functional groups are protonated, which decreases the surface charge and weakens the electrostatic repulsion.

However, the presence of NOM alters the behavior of the NDs as it interacts with the surfaces of the NDs through a combination of electrostatic attraction, hydrogen bonding and hydrophobic interactions, forming a dynamic organic coating. Under acidic conditions, the protonation of functional groups on both NOM and NDs[48] decreases electrostatic stabilization and impairs the steric barriers and hydration layer typically formed by NOM. This destabilization is further facilitated by enhanced attractive interactions such as hydrogen bonding and NOM bridging, which promote particle aggregation.

Under alkaline conditions, the deprotonation of acidic groups on both the ND and NOM surfaces increases their negative surface charge,[48] which enhances electrostatic

repulsion and contributes to stable dispersion. Although a gradual decrease in zeta potential is observed over time in ND–NOM suspensions, possibly due to reorganization of the NOM layer or ion exchange, the DLS results confirm a narrow and stable particle size distribution (Fig. 11b). This apparent discrepancy between the zeta potential and aggregation behavior underscores the crucial role of steric hindrance and hydration layer effects mediated by NOM which remain effective even when the electrostatic repulsion weakens. This emphasizes the robustness of NOM-mediated stabilization of NDs in environmentally relevant alkaline systems.

Such stability is critical not only for their dispersion in applications such as drug delivery systems and the development of nanocomposite materials but also for understanding their interactions in natural ecosystems and their potential for environmental remediation.

An analogous stabilization mechanism is observed in the isotonic balance within biological cells, where the solute concentration outside the cells matches their internal concentration, preventing osmotic pressure changes that could lead to cell damage. Similarly, in riverine or estuary environments, where freshwater mixes with seawater, creating gradients of salinity, organisms have adapted to maintain internal isotonic conditions despite external fluctuations. The NOM coating on NDs suggests that they can maintain their "isotonic" balance under varying environmental conditions, ensuring their stability and preventing aggregation in both highly controlled applications, such as in biomedical devices and under the dynamic conditions typical of river water systems.

4. Conclusions

Our study investigated the behavior of carbon-based nanomaterials in model suspensions designed to mimic environmental conditions. This targeted approach enabled a systematic exploration of the interactions between carbon dots and nanodiamonds and different environmental constituents under controlled laboratory conditions and provided invaluable insights into their behavior and reaction dynamics. While CDs exhibited lower stability and aggregation tendencies, NDs proved to be suitable candidates for experiments with additives.

The latter included the simulation of environmental conditions, such as the riverine environment and the behavior of ND suspensions in the presence of different additives. Under acidic conditions, the addition of bovine serum albumin, fulvic acid, and natural organic substances led to a significant reduction in the absolute zeta potential, although the suspensions remained stable. Conversely, dextran sulfate sodium had a minimal effect on the zeta potential, indicating enhanced electrostatic repulsion between NDs and DSS, leading to stable suspensions in MQ water. In aqueous NaCl solution, all additives, except BSA, increased the absolute zeta potential. While the suspensions in water showed a stable particle size distribution over time,

the suspensions with DSS, FA and NOM formed aggregates in saline solution. Conversely, the suspensions of NDs and NDs with BSA in NaCl solution were unstable over time, indicating strong aggregation and rapid sedimentation.

Furthermore, under alkaline conditions, NOM-coated NDs showed the ability to maintain an "isotonic" equilibrium, highlighting their potential for environmental sustainability. This suggests that these man-made particles remain stable when released into natural ecosystems. Understanding the behavior of NDs, particularly in terms of stability and interaction with natural organic matter, provides the opportunity to exploit their unique properties for environmentally friendly applications ranging from biomedicine to remediation of contaminated sites. Understanding these mechanisms is crucial for the development of strategies to ensure that NDs do not pose unforeseen risks once released into the environment, but can be put to beneficial use.

The presented results, therefore, contribute to our understanding of the complex behavior of carbon-based nanoparticles under environmentally relevant conditions and highlight the importance of considering various environmental factors when assessing their stability and interactions.

Data availability

The data that support the findings of this study are available from the corresponding author, upon reasonable request.

Author contributions

Conceptualization, Ž. F., M. D. S.; methodology, Ž. F., M. D. S., V. K.; software, M. D. S., V. S.; validation, V. S.; formal analysis, D. G., M. P., V. K., V. S.; investigation, D. G., M. P., V. K., V. S.; resources, Ž. F., M. D. S., B. S., S. F.; data curation, Ž. F., D. G., M. D. S., V. S.; writing – original draft preparation, Ž. F., M. D. S., V. K.; writing – review and editing, B. S., D. G., V. K., V. S., S. F.; visualization, Ž. F., M. D. S.; supervision, Ž. F.; project administration, Ž. F., M. D. S.; funding acquisition, Ž. F., M. D. S. All authors have read and agreed to the published version of the manuscript.

Conflicts of interest

There are no conflicts of interest to declare.

Acknowledgements

References

1 J. Gao, M. Zhu, H. Huang, Y. Liu and Z. Kang, Advances, challenges and promises of carbon dots, *Inorg. Chem. Front.*, 2017, **4**, 1963–1986, DOI: **10.1039/C7QI00614D**.

2 S. Xiang and M. Tan, Carbon dots derived from natural sources and their biological and environmental impacts, *Environ. Sci.: Nano*, 2022, **9**, 3206–3225, DOI: **10.1039/D2EN00435F**.

3 T. Das, B. K. Saikia, H. P. Dekaboruah, M. Bordoloi, D. Neog, J. J. Bora and D. Ramaiah, Blue-fluorescent and biocompatible carbon dots derived from abundant low-quality coals, *J. Photochem. Photobiol., B*, 2019, **195**, 1–11, DOI: **10.1016/j.jphotobiol.2019.04.004**.

4 X. Zheng, K. Qin, L. He, Y. Ding, Q. Luo, C. Zhang, X. Cui, Y. Tan, L. Li and Y. Wei, Novel fluorescent nitrogen-doped carbon dots derived from Panax notoginseng for bioimaging and high selectivity detection of Cr^{6+}, *Analyst*, 2021, **146**, 911–919, DOI: **10.1039/D0AN01599G**.

5 V. N. Mochalin, O. Shenderova, D. Ho and Y. Gogotsi, The properties and applications of nanodiamonds, *Nat. Nanotechnol.*, 2012, **7**, 11–23, DOI: **10.1038/nnano.2011.209**.

6 Y. K. Tzeng, O. Faklaris, B. M. Chang, Y. Kuo, J. H. Hsu and H. C. Chang, Superresolution imaging of albumin-conjugated fluorescent nanodiamonds in cells by stimulated emission depletion, *Angew. Chem., Int. Ed.*, 2011, **50**(10), 2262–2265.

7 H. Kato, A. Nakamura, M. Horie, S. Endoh, K. Fujita, H. Iwahashi and S. Kinugasa, Preparation and characterization of stable dispersions of carbon black and nanodiamond in culture medium for in vitro toxicity assessment, *Carbon*, 2011, **49**(12), 3989–3997, DOI: **10.1016/j.carbon.2011.05.039**.

8 S. Pedroso-Santana, A. Sarabia-Saínz, N. Fleitas-Salazar, K. Santacruz-Gómez, M. Acosta-Elías, M. Pedroza-Montero and R. Riera, Deagglomeration and characterization of detonation nanodiamonds for biomedical applications, *J. Appl. Biomed.*, 2017, **15**(1), 15–21, DOI: **10.1016/j.jab.2016.09.003**.

9 B. M. Chang, L. Pan and H. H. Lin, *et al.*, Nanodiamond-supported silver nanoparticles as potent and safe antibacterial agents, *Sci. Rep.*, 2019, **9**, 13164, DOI: **10.1038/s41598-019-49675-z**.

10 P. Aprà, L. Mino, A. Battiato, P. Olivero, S. Sturari, M. C. Valsania, V. Varzi and F. Picollo, Interaction of nanodiamonds with water: Impact of surface chemistry on hydrophilicity, aggregation, and electrical properties, *Nanomaterials*, 2021, **11**, 2740, DOI: **10.3390/nano11102740**.

11 M. Aramesh, O. Shimoni, K. Ostrikov, S. Prawer and J. Cervenka, Surface charge effects in protein adsorption on nanodiamonds, *Nanoscale*, 2015, **7**(13), 5726–5736, DOI: **10.1039/c5nr00250h**.

12 T. Skaltsas, S. Pispas and N. Tagmatarchis, Non-covalent nanodiamond–polymer dispersions and electrostatic immobilization of bovine serum albumin protein, *Mater. Res. Express*, 2015, **2**, 115005, DOI: **10.1088/2053-1591/2/11/115005**.

13 W. W. Tang, *et al.*, Impact of humic/fulvic acid on the removal of heavy metals from aqueous solutions using nanomaterials: A review, *Sci. Total Environ.*, 2014, **468–469**, 1014–1027, DOI: **10.1016/j.scitotenv.2013.09.044**.

3918 | *Environ. Sci.: Nano*, 2025, **12**, 3904–3920

This journal is © The Royal Society of Chemistry 2025

14 X. Luo, Y. Zhang, Y. Wang, Q. Chen, J. Tu, M. He, J. Zhang and Y. Wu, Exploring the environmental factor fulvic acid attenuates the ecotoxicity of graphene oxide under food delivery exposure, *Ecotoxicol. Environ. Saf.*, 2024, **270**, 115893, DOI: **10.1016/j.ecoenv.2023.115893**.

15 A. Shirani, N. Nunn, O. Shenderova, E. Osawa and D. Berman, Nanodiamonds for improving lubrication of titanium surfaces in simulated body fluid, *Carbon*, 2019, **143**, 890–896, DOI: **10.1016/j.carbon.2018.12.005**.

16 J. Mariam, P. M. Dongre and D. C. Kothari, Study of interaction of silver nanoparticles with bovine serum albumin using fluorescence spectroscopy, *J. Fluoresc.*, 2011, **8**, 2193–2199, DOI: **10.1007/s10895-011-0922-3**.

17 J. Kwon, C. Lee and S. Heo, *et al.*, DSS-induced colitis is associated with adipose tissue dysfunction and disrupted hepatic lipid metabolism leading to hepatosteatosis and dyslipidemia in mice, *Sci. Rep.*, 2021, **11**, 5283, DOI: **10.1038/s41598-021-84761-1**.

18 R. G. Qualls and B. L. Haines, Biodegradability of dissolved organic matter in forest throughfall, soil solution, and stream water, *Soil Sci. Soc. Am. J.*, 1992, **56**(2), 578–586, DOI: **10.2136/sssaj1992.03615995005600020038x**.

19 T. G. Reyes and J. M. Crisosto, Characterization of dissolved organic matter in river water by conventional methods and direct sample analysis-time of flight-mass spectrometry, *J. Chem.*, 2016, **2016**, 1–11, DOI: **10.1155/2016/1537370**.

20 S. Mohapatra, N. Sharma, G. Mohapatra, L. P. Padhye and S. Mukherji, Seasonal variation in fluorescence characteristics of dissolved organic matter in wastewater and identification of proteins through HRLC-MS/MS, *J. Hazard. Mater.*, 2021, **413**, 125453, DOI: **10.1016/j.jhazmat.2021.125453**.

21 A. Kathiravan and R. Renganathan, Interaction of colloidal TiO_2 with bovine serum albumin: A fluorescence quenching study, *Colloids Surf., A*, 2008, **324**, 176–180, DOI: **10.1016/j.colsurfa.2008.04.017**.

22 W. Zhang, Q. Zhang and F. Wang, *et al.*, Comparison of interactions between human serum albumin and silver nanoparticles of different sizes using spectroscopic methods, *Biopolymers*, 2015, **30**(4), 397–404, DOI: **10.1002/bio.2748**.

23 T. Petit and L. j. Puskar, FTIR spectroscopy of nanodiamonds: Methods and interpretation, *Diamond Relat. Mater.*, 2018, **89**, 52–66, DOI: **10.1016/j.diamond.2018.08.005**.

24 K. Chen, S. Mylon and M. Elimelech, Aggregation kinetics of alginate-coated hematite nanoparticles in monovalent and divalent electrolytes, *Environ. Sci. Technol.*, 2006, **40**(5), 1516–1523, DOI: **10.1021/ES0518068**.

25 K. Huynh and K. Chen, Aggregation kinetics of citrate and polyvinylpyrrolidone coated silver nanoparticles in monovalent and divalent electrolyte solutions, *Environ. Sci. Technol.*, 2011, **45**(13), 5564–5571, DOI: **10.1021/es200157h**.

26 D. Saha, S. Kumar, J. P. Mata, A. E. Whitten and V. K. Aswal, Competitive effects of salt and surfactant on the structure of nanoparticles in a binary system of nanoparticle and protein, *Phys. Chem. Chem. Phys.*, 2023, **25**(33), 22130–22144, DOI: **10.1039/d3cp02619a**.

27 M. Elimelech, *Particle Deposition and Aggregation: Measurement, Modelling, and Simulation*, Butterworth-Heinemann, Woburn, 1998.

28 N. Akaighe, S. W. Depner, S. Banerjee, V. K. Sharma and M. Sohn, The effects of monovalent and divalent cations on the stability of silver nanoparticles formed from direct reduction of silver ions by Suwannee River humic acid/natural organic matter, *Sci. Total Environ.*, 2012, **441**, 277–289, DOI: **10.1016/j.scitotenv.2012.09.055**.

29 M. Paloncýová, M. Langer and M. Otyepka, Structural dynamics of carbon dots in water and N,N-dimethylformamide probed by all-atom molecular dynamics simulations, *J. Chem. Theory Comput.*, 2018, **14**(4), 2076–2083, DOI: **10.1021/acs.jctc.7b01149**.

30 Z. Ge and Y. Wang, Estimation of nanodiamond surface charge density from zeta potential and molecular dynamics simulations, *J. Phys. Chem. B*, 2017, **121**, 3394–3402.

31 Z. Liu, D. Leininger, A. Koolivand, A. I. Smirnov, O. Shenderova, D. W. Brenner and J. Krim, Tribological properties of nanodiamonds in aqueous suspensions: Effect of the surface charge, *RSC Adv.*, 2015, **5**, 78933–78940, DOI: **10.1039/c5ra14151f**.

32 J. Li, W. Cao, Y. Shu, H. Zhang, X. Qian, X. Kong, L. Wang and X. Peng, Water molecules bonded to the carboxylate groups at the inorganic–organic interface of an inorganic nanocrystal coated with alkanoate ligands, *Natl. Sci. Rev.*, 2022, **9**(2), nwab138, DOI: **10.1093/nsr/nwab138**.

33 P. G. Squire, P. Moser and C. T. O'Konski, Hydrodynamic properties of dextrans in solution, *J. Phys. Chem.*, 1968, **72**(11), 3924–3930.

34 N. Varga, V. Hornok, D. Sebők and I. Dékány, Comprehensive study on the structure of BSA from extended-to-aged form in wide (2–12) pH range, *Int. J. Biol. Macromol.*, 2016, **88**, 51–58, DOI: **10.1016/j.ijbiomac.2016.03.030**.

35 Y. V. Kulvelis, A. V. Shvidchenko, A. E. Aleksenskii, E. B. Yudina, V. T. Lebedev, M. S. Shestakov, A. T. Dideikin, L. O. Khozyaeva, A. I. Kuklin, G. y. Török, M. I. Rulev and A. Y. Vul, Stabilization of detonation nanodiamonds hydrosol in physiological media with poly(vinylpyrrolidone), *Diamond Relat. Mater.*, 2018, **87**, 78–89, DOI: **10.1016/j.diamond.2018.05.012**.

36 B. Zhu, D. Salazar and P. Willems, Impacts of external factors on salinity patterns via numerical modeling along the Scheldt Estuary, Belgium, *J. Hydrol. Reg. Stud.*, 2024, **52**, 102026, DOI: **10.1016/j.ejrh.2024.102026**.

37 H.-D. Wang, C. H. Niu, Q. Yang and I. Badea, Study on protein conformation and adsorption behaviors in nanodiamond particle–protein complexes, *Nanotechnology*, 2011, **22**(14), 145703, DOI: **10.1088/0957-4484/22/14/145703**.

38 T.-C. Yang, C.-Y. Chang, A. A. Yarmishyn, Y.-S. Mao, Y.-P. Yang, M.-L. Wang, C.-C. Hsu, H.-Y. Yang, D.-K. Hwang, S.-J. Chen, M.-L. Tsai, Y.-H. Lai, Y. Tzeng, C.-C. Chang and S.-H. Chiou, Carboxylated nanodiamond-mediated CRISPR-Cas9 delivery of human retinoschisis mutation into human iPSCs

This journal is © The Royal Society of Chemistry 2025

Environ. Sci.: Nano, 2025, **12**, 3904–3920 | 3919

and mouse retina, *Acta Biomater.*, 2020, **101**, 484–494, DOI: **10.1016/j.actbio.2019.10.037**.

39 B. Porsch and L. Sundelöf, Size-exclusion chromatography and dynamic light scattering of dextrans in water: Explanation of ion-exclusion behaviour, *J. Chromatogr. A*, 1994, **669**, 21–30, DOI: **10.1016/0021-9673(94)80333-1**.

40 O. A. Madkhali, S. S. Moni and M. H. Sultan, Formulation and evaluation of injectable dextran sulfate sodium nanoparticles as a potent antibacterial agent, *Sci. Rep.*, 2021, **11**, 9914, DOI: **10.1038/s41598-021-89330-0**.

41 C. Konstantinou, G. Biscontin, N. J. Jiang and K. Soga, Application of microbially induced carbonate precipitation to form bio-cemented artificial sandstone, *J. Rock Mech. Geotech. Eng.*, 2021, **13**(3), 579–592, DOI: **10.1016/j.jrmge.2021.01.010**.

42 V. Kamchoom, T. Khattiwong, T. Treebupachatsakul, S. Keawsawasvong and A. K. Leung, Spatiotemporal variations of sand hydraulic conductivity by microbial application methods, *J. Rock Mech. Geotech. Eng.*, 2024, **16**(1), 268–278, DOI: **10.1016/j.jrmge.2023.04.024**.

43 K. L. Chen and M. Elimelech, Influence of humic acid on the aggregation kinetics of fullerene (C_{60}) nanoparticles in monovalent and divalent electrolyte solutions, *J. Colloid Interface Sci.*, 2007, **309**(1), 126–134, DOI: **10.1016/j.jcis.2007.01.074**.

44 M. G. Chernysheva, I. Y. Myasnikov, G. A. Badun, D. N. Matorin, D. T. Gabbasova, A. I. Konstantinov and N. A. Kulikova, Humic substances alter the uptake and toxicity of nanodiamonds in wheat seedlings, *J. Soils Sediments*, 2016, **18**(4), 1335–1346, DOI: **10.1007/s11368-016-1564-5**.

45 Y. X. Zhang, W. J. Zhang, Y. Fedutik, Z. W. Mao and C. Y. Gao, Nanodiamonds of different surface chemistry influence the toxicity and differentiation of rat bone mesenchymal stem cells in vitro, *J. Nanosci. Nanotechnol.*, 2019, **19**(9), 5426–5434, DOI: **10.1166/jnn.2019.16545**.

46 S. Pandit and S. Kundu, Fluorescence quenching and related interactions among globular proteins (BSA and lysozyme) in presence of titanium dioxide nanoparticles, *Colloids Surf., A*, 2021, **628**, 127253, DOI: **10.1016/j.colsurfa.2021.127253**.

47 J.-C. Arnault, Surface modifications of nanodiamonds and current issues for their biomedical applications, in *Novel Aspects of Diamond – From Growth to Applications, Topics in Applied Physics*, ed. N. Yang, Springer Verlag, 2015, vol. 121, pp. 85–122, DOI: **10.1007/978-3-319-09834-0_4**.

48 R. D. Vogt, Ø. A. Garmo, K. Austnes, Ø. Kaste, S. Haaland, J. E. Sample, J.-E. Thrane, L. B. Skancke, C. B. Gundersen and H. A. de Wit, Factors governing site and charge density of dissolved natural organic matter, *Water*, 2024, **16**(12), 1716, DOI: **10.3390/w16121716**.

3920 | *Environ. Sci.: Nano*, 2025, **12**, 3904–3920

This journal is © The Royal Society of Chemistry 2025